Fracture simulation of partially threaded bolts under tensile loading

Yang, Fei; Veljkovic, Milan; Liu, Yuqing

DOI
10.1016/j.engstruct.2020.111373

Publication date
2021

Document Version
Final published version

Published in
Engineering Structures

Engineering Structures 226 (2021) 111373

Contents lists available at ScienceDirect

Engineering Structures

journal homepage: www.elsevier.com/locate/engstruct

Fracture simulation of partially threaded bolts under tensile loading

Fei Yang [a,b], Milan Veljkovic [b], Yuqing Liu [a,*]

[a] Department of Bridge Engineering, Tongji University, Shanghai, China
[b] Department of Engineering Structures, Delft University of Technology, Delft, the Netherlands

ARTICLE INFO

Keywords:
Partially threaded bolt
Bolted connection
Post-necking stress–strain
Void grow model (VGM)
Thread stripping
Thread rolling

ABSTRACT

Failure of bolts exposed to tension is generally avoided in the design of bolted connections due to the smaller deformation capacity of bolts than the connected plates. This is one of the reasons why few studies focus on the tensile failure behaviour of bolts. However, failure behaviour of bolts is essential for the advanced finite element analysis especially relevant to the deformation capacity and failure mode of bolted connections. This paper presents a numerical study on the fracture of partially threaded bolts under tension incorporating damage models, with which the failure mechanism of bolts can be better understood. The post-necking stress–strain relation is firstly calibrated to describe the behaviour of bolt threaded parts at large deformation. Then, direct tension tests on partially threaded bolts with different threaded lengths within the grip are modelled using ABAQUS with the explicit solver. Two criteria for fracture are investigated: the void growth model (VGM) and a model proposed by Bao and Wierzbicki (BW). The former is adopted to simulate the tensile fracture of bolts and the latter is used to predict the thread stripping failure. Results indicate that bolt failure modes of tensile fracture and thread stripping can be well predicted by combining the calibrated post-necking stress–strain relation and a suitable fracture criterion in the analysis. It is revealed that the large plastic strain in the threads introduced by thread rolling process is a major reason for the thread stripping failure.

1. Introduction

For the design of a bolted end-plate connection in beam-column joints, its moment resistance and rotational stiffness can be predicted according to the component method proposed in EN 1993-1-8 [1]. The joint could be assumed to have sufficient rotation capacity for plastic analysis, provided that the moment resistance is governed by column flange in bending or beam end-plate in bending rather than the failure of bolts exposed to tension. Hence, failure of bolts exposed to tension is generally avoided in the design of bolted connections due to the smaller deformation capacity than the connected plates. In addition, it seems difficult to estimate the ultimate rotation capacity for an end-plate connection theoretically, as the deforming behaviour of each component has not been investigated in depth. For the simple case of bolts under tensile loading, the deformation capacity is commonly considered to be relatively small and the failure is only recognized much less ductile than the connected plates. However, for the advanced finite element analysis of bolted connection especially relevant to the deformation capacity and failure mode, the failure behaviour of bolts exposed to tension needs to be considered in detail.

In the experiments conducted by Coelho et al. [2], it was observed that bolt failure including tensile fracture and thread stripping would govern the final failure of an extended end-plate connection. In the experiments conducted by Grimsmo et al. [3], end-plate connections were devised with an intended end-plate bending deformation combining with bolt tensile fracture. It was observed that using one nut per bolt led to thread stripping failure and two nuts led to bolt tensile fracture. Two nuts per bolt produced a larger moment resistance and two times rotation capacity compared to one nut per bolt in the connections. Accordingly, it is necessary to investigate the deforming behaviour of bolts to provide insights into the failure process of bolted connections.

In the tests conducted by Moore et al. [4], a total of 1533 structural bolts, consisting of four strength grades and six diameters, were tested in direct tension and shear to investigate the tensile and shear strength of structural bolts. In the last part of the report [4], it was indicated that the ductility of high-strength bolts would depend on the number of threads included in the grip length, and equations to predict the stiffness and ductility of high-strength bolts under tension would be very useful. Renner and Lange [5] experimentally investigated the load-bearing behaviour of high-strength bolts in combined tension and shear. It was

* Corresponding author.
E-mail address: yql@tongji.edu.cn (Y. Liu).

https://doi.org/10.1016/j.engstruct.2020.111373
Received 6 May 2020; Received in revised form 14 August 2020; Accepted 25 September 2020
Available online 17 October 2020

deduced that the ductility of the base material might play a bigger role in the load-bearing behaviour under combined tension and shear, as bolts grade 4.6 had a larger ratio of shear strength to tensile strength than bolts grade 8.8.

In terms of the bolt deforming behaviour, Fransplass et al. [6] studied the behaviour of threaded rods at elevated strain rates. Two failure modes including thread stripping and tensile fracture were observed in tests. The threaded assembly tests showed that the number of threads within the grip could alter the failure mode. A short grip length would lead to the reduction of thread shear area because diffuse necking occurred in thread engagement length. Grimsmo et al. [7] experimentally and numerically investigated the failure behaviour of M16 bolt (grade 8.8) and nut assemblies under tensile loading. It was found that threaded length within the grip of partially threaded bolts governed the failure mode of bolt assemblies. If the threaded length within the grip is less than the bolt diameter, the failure mode would be thread stripping, which is a rather brittle failure and should be avoided in practise. Although the failure mode of partially threaded bolts under tensile loading has been investigated experimentally and numerically, the failure mechanisms, especially for the thread stripping failure, are still needed to be studied further.

For the numerical analysis, it is becoming prevailing to incorporate damage model into the finite element analysis (FEA) of steel structures [7–10]. For example, Amadio et al. [10] recently proposed a refined finite element modelling approach to predicting structural behaviour of steel-concrete composite welded joints under cyclic loadings. The micromechanics-based GTN plasticity model is used to simulate the damage of steel plate in the welded joint. The numerical predictions agree well with the experimental results both in terms of global and local behaviours. Generally, two major mechanisms cause steel to fracture, which are ductile fracture due to the nucleation, growth, and coalescence of voids, and shear fracture due to shear band localization [11–13]. Therefore, it is worth implementing the fracture simulation for bolts under tensile loading to check the applicability of steel damage models and explain the bolt fracture mechanism.

The objective of this paper is to present a numerical method to simulate the fracture of partially threaded bolts and provide insights into the fracture mechanism of bolts under tensile loading. This research is relevant for example, in bolted beam-column connection especially when high-strength steel is used and in pretension connection in bridges and in towers supporting wind turbines because of evidence of over-tightening. Direct tension tests on M16 grade 8.8 partially threaded bolts are analysed based on the experimental results reported in [7]. Post-necking stress-strain relation of the bolts is calibrated based on the combined linear and power stress-strain law. Two criteria for fracture, the void growth model (VGM) [14–17] and a model proposed by Bao and Wierzbicki (BW) [18,19], are adopted to simulate the fracture of the bolts with different threaded lengths in the grip.

2. Finite element models

2.1. Available tension tests

In the direct tension tests conducted by Grimsmo et al. [7], 7 groups of partially threaded bolts with different threaded lengths within the grip and 2 groups of fully threaded bolts were tested to examine the tensile behaviour especially for the failure mode of bolt assemblies. It shows that fully threaded bolts have larger deformation capacity with bolt tensile fracture failure. Partially threaded bolts have two distinct failure modes including thread stripping failure and tensile fracture failure. The former is a brittle failure and the latter has a certain ductility. Dimensions of the partially threaded bolt assemblies in the study by Grimsmo et al. [7] are shown in Fig. 1. The bolts are M16 × 160 mm of grade 8.8 manufactured according to ISO 4014 [20]. Property class of the nuts is 8 manufactured according to ISO 4032 [21]. The unthreaded length for M16 bolt is 113 mm and the threaded length is 47 mm. Five tension tests with grip lengths 118, 122, 126, 130, and 141 mm are selected in this paper to numerically study the failure mechanism of partially threaded bolts under tensile loading. The threaded lengths within the grip are 5, 9, 13, 17, and 28 mm, respectively, as shown in Fig. 1.

An equivalent tensile loading model shown in Fig. 2 is used in this paper to simulate the actual tests, since a part of deformation of the test set-up is included in the measured displacement. The equivalent loading model consists of a M16 × 80 bolt and an elastic spring connected to bolt head. The elastic spring is introduced to account on the elastic deformation of the test set-up and the reduced 80 mm bolt shank. Considering the deformation of a bolt assembly, expressed by Eq. (1.1), tensile stiffness of the elastic spring is estimated by Eq. (1.2).

$$\text{Deformation} = \frac{T}{k_t} = \frac{T}{k_s} + \frac{T}{k_b} \tag{1.1}$$

$$k_s = \frac{k_b k_t}{k_b - k_t} \tag{1.2}$$

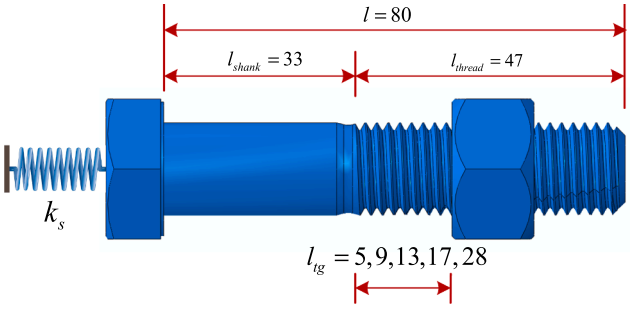

Fig. 2. Equivalent tensile loading model for numerical analyses.

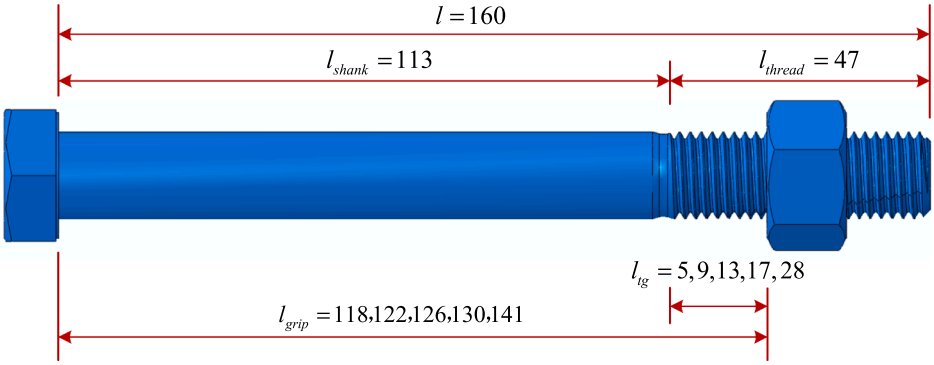

Fig. 1. Dimensions of partially threaded bolt assemblies (according to [7]).

In Eq. (1), T is the force in tension; k_s, k_b, and k_t denote spring stiffness, bolt tensile stiffness, and experimental tensile stiffness, respectively. According to the following calculations, tensile stiffness of the simulated M16 × 80 bolts can be acquired. Combining the experimental tensile stiffness of bolt assemblies, tensile stiffness of the elastic spring k_s could be estimated. It is taken as 60 kN/mm for the analysis in this paper.

2.2. Geometric dimensions

Dimensions of bolt and nut threads are of significance for simulation of bolt assemblies, which may have a major impact on failure mode and deformation capacity of bolt assemblies. In the study by Grimsmo et al. [7], actual dimensions of bolt and nut threads were measured and reported, as illustrated in Fig. 3. Major diameters for bolt and nut threads are 16.36 mm and 15.88 mm, respectively. Minor diameters for bolt and nut threads are 14.05 mm and 13.36 mm, respectively. The measured pitch is 2.0 mm and the measured nut height is 14.2 mm [22]. The hole of the nut has a "bell-mouth" configuration as reported in [7]. This configuration leads to only three threads in the nut with a full height and other threads with a reduced height, which would affect the tensile behaviour due to the reduction of shear area of bolt threads. The "bell-mouth" configuration is realized in the modelling as shown in Fig. 3, according to the measured dimensions listed in appendix C of [22].

2.3. Finite element modelling

Five numerically investigated tension tests are denoted as Tension118, Tension122, Tension126, Tension130, and Tension141. The number stands for grip lengths in the actual tests. Fig. 4 shows the configuration of Tension130 test modelled based on ABAQUS [23]. There are four parts in the finite element model including a bolt, a nut, a circular steel plate, and an elastic spring. As shown in Fig. 4a, the lower end of the elastic spring is connected to a reference point, which is coupled to the bolt top surface and constrained in X and Z directions. A vertical displacement is applied on the upper end of the elastic spring to realize the tensile loading with a displacement control method. Translational freedoms of the steel plate top surface are constrained, thereby the vertical movement of the nut top surface is restrained. General contact is used to model the contact property between circular steel plate and nut top surface and between the threads of bolt and nut. The normal behaviour in the general contact is modelled using "hard" contact in ABAQUS [23], while the tangential behaviour is modelled using "penalty" friction formulation with "friction coefficient" equal to 0.2. Values of the friction coefficient depend on the treatment of friction surfaces, which are defined in EN 1090-2 [24]. The friction coefficient corresponding to Class D, which is surfaces as rolled, is equal to 0.2. Therefore, the "friction coefficient" in the numerical analysis is set to 0.2 for bolt and nut assemblies as their surfaces are as rolled in the tests.

Fig. 4b illustrates the mesh of the Tension130 model. For the steel plate above the nut, its mesh size is set to 1.5 mm with element type C3D8R. This plate is modelled as an elastic material with modulus of elasticity equal to 210 GPa. For the bolt and nut, a 10-node modified quadratic tetrahedron C3D10M element is adopted to realize the free mesh for threaded parts of the bolt and nut. The quadratic element yields relatively accurate numerical results. Element size for unthreaded part of the bolt is set to 1.5 mm, while for threaded part it is 0.5 mm. Element size for the nut is 0.8 mm. Fig. 4c shows the bolt detailed geometric configuration from unthreaded part to threaded part, which is a gradual transition as in a real bolt to make the stress transfer smooth. This transition is essential for bolt simulation especially for bolts with a short-threaded length within the grip. An unrealistic transition may result in a failure initiated from the transition region. Fig. 4e shows the engagement of bolt and nut, where clearance between bolt threads and nut threads can be clearly seen. A larger clearance would reduce shear area of the threads, thereby tensile strength, ductility, and failure mode of bolts may be altered. In this paper, the fracture mechanism of bolts under tensile loading will be investigated based on the measured dimensions of bolt and nut threads. Effects of thread clearances on bolt tensile behaviour are not included.

3. Material properties

3.1. Pre-necking properties

Tensile coupon tests were performed on specimens machined from M16 partially threaded (PT) and fully threaded (FT) bolts to specimens with a reduced diameter of 12 mm [7]. Since the machined part in PT bolt specimen locates in unthreaded part of the bolts, the measured engineering stress-strain curves for PT bolts only represent the behaviour of unthreaded part, whereas the measured engineering stress-strain curves for FT bolts represent the behaviour of threaded part. The stress-strain behaviour of threaded part of PT bolts is slightly different from the corresponding unthreaded part, because thread rolling process for producing the external threads of bolts introduces large plastic strain in the threaded region, as analysed in [25–28]. Effects of thread rolling process on thread failure behaviour will be discussed in the following analysis.

In the numerical analysis, true stress-strain relation needs to be input. The pre-necking true stress-strain relation can be converted from the pre-necking engineering stress-strain curve measured in tensile coupon tests. Eqs. (2.1) and (2.2) is the conversion equations.

$$\varepsilon_t = ln(1+\varepsilon_e) \tag{2.1}$$

$$\sigma_t = \sigma_e(1+\varepsilon_e) \tag{2.2}$$

In Eq. (2), σ_e, ε_e represent the engineering stress and strain; σ_t, ε_t denote the true stress and strain. Fig. 5 shows the measured engineering stress-strain curves and the converted true stress-strain curves based on Eq. (2) for PT and FT bolts before the onset of necking. As shown in Fig. 5, the true stress will be much larger than the engineering stress with the increase of engineering strain for the same material. Yield and ultimate strengths of PT bolts are higher than those of FT bolts. The engineering strain corresponding to ultimate strength of FT and PT bolts is 0.07 and 0.065, respectively, indicating that the FT bolts have a larger tensile deformation capacity than PT bolts at least at the uniform deforming stage.

Apart from tensile coupon tests, hardness tests were also conducted for PT and FT bolts on their threaded parts [7]. The average hardness

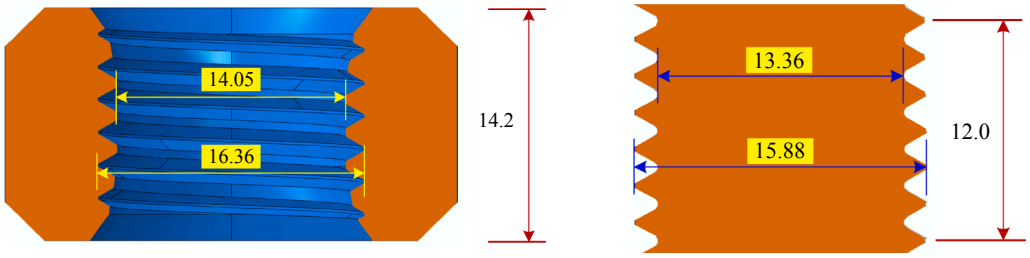

Fig. 3. Measured dimensions of nut and bolt threads (according to [7,22]).

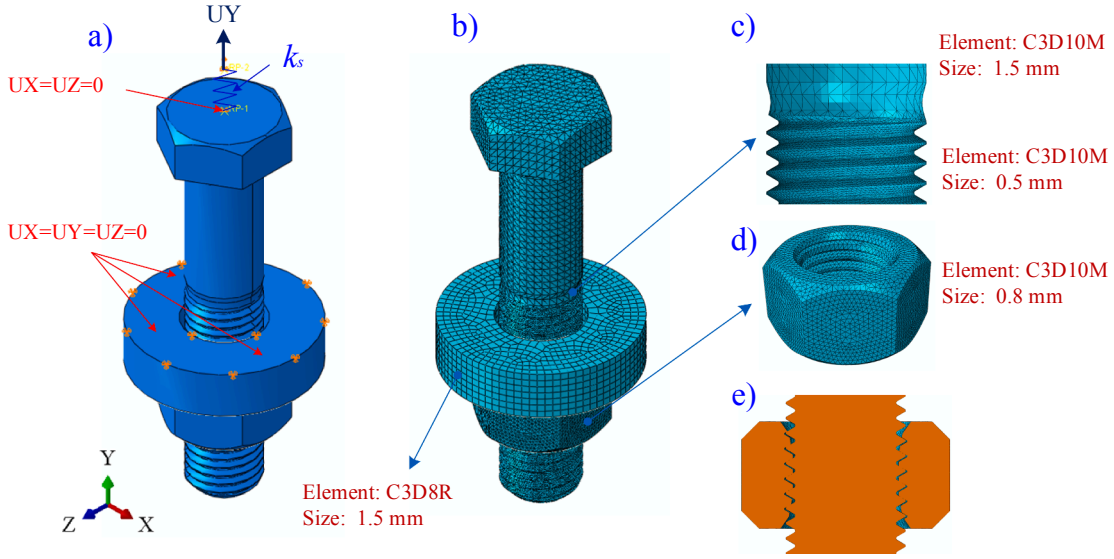

Fig. 4. FE model illustration (Configuration for Tension130 test modelling).

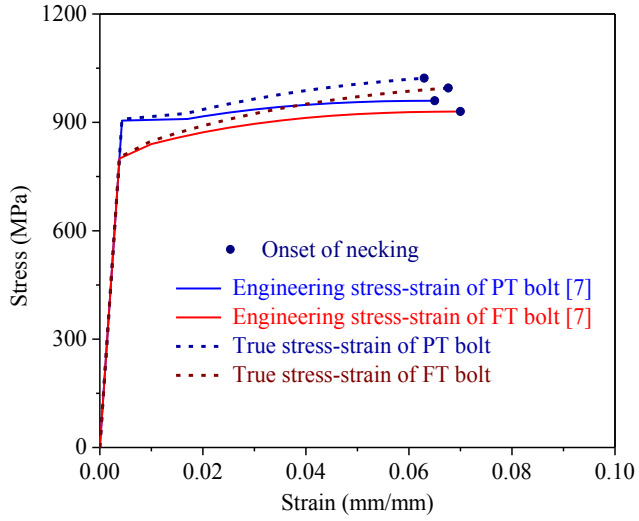

Fig. 5. Pre-necking engineering and true stress–strain curves of PT and FT bolts.

values were 301 HV and 293 HV for PT and FT bolts, respectively. The hardness of threaded part of PT bolts is about 3% higher than that of FT bolts. The hardness of a material is commonly assumed proportional to its yield strength. However, the yield strength of PT bolts, measured from bolt unthreaded part, is 14% higher than that of FT bolts. Accordingly, it is assumed here the stress-strain relation for threaded part of PT bolts is closer to the measured relation of FT bolts. The rationality will be proved in the following calibrations of the material properties.

3.2. Post-necking properties

The post-necking true stress-strain relation cannot be directly derived from the engineering stress-strain curves due to the strain localization effect. Ling [29] proposed a combined linear and power post-necking true stress-strain relations, which could be calibrated just using a weighting factor W for the investigated metallic material, as expressed in Eq. (3). The expression is extended by Yang and Veljkovic [30,31] to describe post-necking degraded stress-strain relation of high-strength steels with a weighting factor W less than zero.

$$\sigma_t = (W)(a\varepsilon_t + b) + (1 - W)\left(K\varepsilon_t^n\right) \tag{3}$$

In Eq. (3), $a = \sigma_{t,u}$, $n = \varepsilon_{t,u}$, $b = a(1-n)$, $K = a/n^n$,. $\sigma_{t,u}$ and $\varepsilon_{t,u}$ denote the true stress and true strain at the onset of necking, respectively.

Fig. 6 shows the true stress-strain relations for PT and FT bolts described by the combined linear and power law of Eq. (3), in which weighting factor W is set to 0.2, 0, and −0.2 for FT bolts and 0 for PT bolts. The post-necking stress for FT bolts is increasing with the increase of plastic strain when W is larger than zero, as shown in Fig. 6a, and the post-necking stress will slightly decrease when W is equal to −0.2. A full range stress-strain relation till fracture for PT bolts is proposed in [7] with four calibrated parameters, as expressed in Eq. (4).

$$\sigma_t = \sigma_y + \sum_{i=1}^{2} Q_i\left(1 - exp\left(-\frac{\theta_i}{Q_i}\left(\varepsilon_p - \varepsilon_{p,plat}\right)\right)\right) \tag{4}$$

In Eq. (4), σ_y is the yield stress; Q_i and θ_i are the hardening constants of the extended Voce hardening rule; ε_p is the equivalent plastic strain; and $\varepsilon_{p,plat}$ is the equivalent plastic strain at the end of the yield plateau. The true stress–strain relation by Eq. (4) is illustrated in Fig. 6b and compared to the combined linear and power relations expressed by Eq. (3). The post-necking true stress–strain described by Eq. (3) with $W = 0$ is close to the relation by Eq. (4) when plastic strain is less than 0.5. For larger plastic strain, Eq. (4) provides slightly larger true stress. For the material property of the nut, its true stress is taken as 0.8 times of the true stress of FT bolts at the same plastic strain, as the measured hardness value for the nut is about 0.8 times of that for FT bolts.

3.3. Calibration of the material properties

Material properties of PT bolts are calibrated according to the direct tension experimental results of PT bolts. Quasi-static numerical analyses on Tension130 and Tension141 tests are carried out to calibrate the bolt material properties using the explicit solver in ABAQUS [23]. The target time increment is set to 0.002 s and the duration of the tensile step is 200 s. Mises criterion is employed to describe the yield surfaces with the associated plastic flow. The numerical tension-displacement curves are obtained by postprocessing the force in tension and displacement occurred in the upper end of the spring, as shown in Fig. 4a. For Tension130 test, material properties are input as the true stress–strain relation based on the measured properties of PT bolts. Its post-necking stress–strain relation is described by Eq. (3) with W equal to zero, as

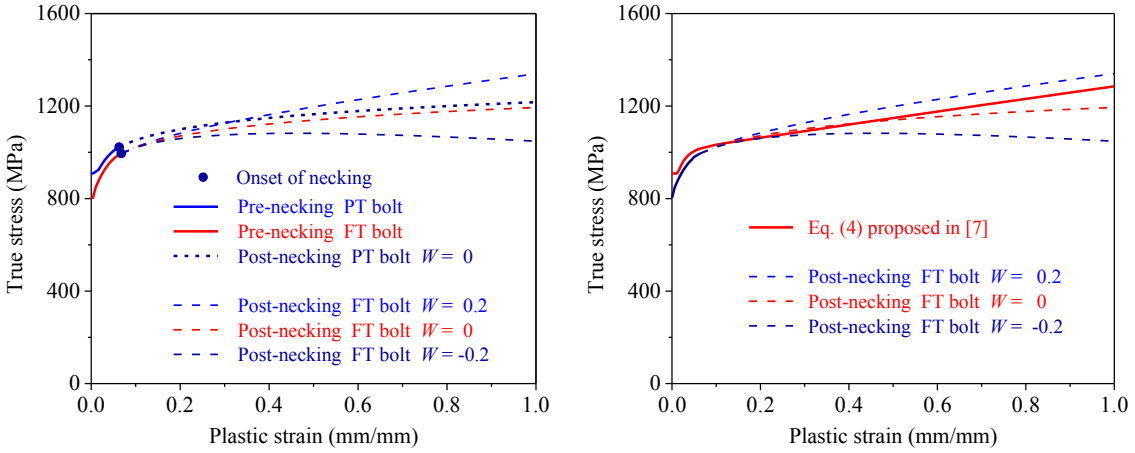

a) Stress-strain for the PT and FT bolts b) Stress-strain compared with the proposed curve

Fig. 6. True stress–strain curves for PT and FT bolts.

shown in Fig. 6a. The numerical tension-displacement curve compared to the experimental result are shown in Fig. 7. The initial tensile stiffness and the decreasing trend at the load-descending stage is well predicted. However, the tension in the non-linear stage is slightly overestimated compared to the experimental result. It could be inferred therefore that the measured tensile strength from the unthreaded part of PT bolts would be slightly larger than the actual average strength in the threaded part of PT bolts due to the thread rolling process.

Material properties based on the measured pre-necking behaviour of FT bolts and the combined linear and power post-necking behaviour with weighting factor equal to 0.2, 0, and −0.2, as shown in Fig. 6a, are analysed for Tension130 model. Fig. 8a presents the numerical tension-displacement curves compared to the experimental results of Tension130 test. It can be concluded that using weighting factor $W = 0$ gives the closest prediction to the experimental result for Tension130 test. Clearly, a larger weighting factor would result in a relatively larger tension at the load-descending stage. For Tension141 test, as shown in Fig. 8b, post-necking properties with weighting factor $W = 0$ also give a good prediction for the descending stage of the experimental tension-displacement curve. Consequently, it is considered that the bolt post-necking behaviour can be well described using the combined linear and power stress–strain relation with weighting factor $W = 0$.

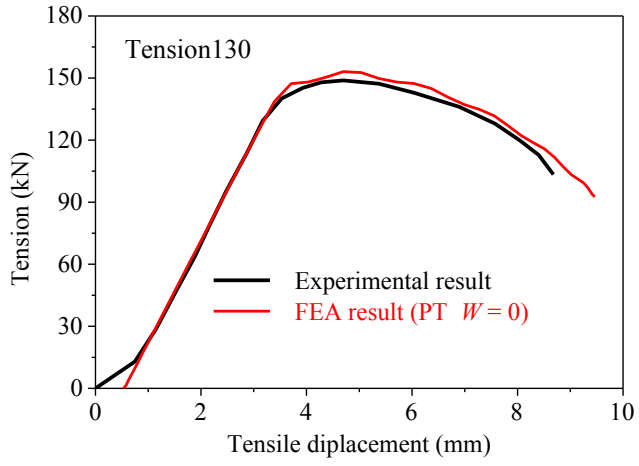

Fig. 7. Numerical tension-displacement curve compared to experimental result for Tension130.

4. Calibration of the fracture criteria

4.1. RT fracture criterion

Using the full-range true stress–strain relation of bolts including the calibrated post-necking stress–strain relation, the elastic and plastic behaviour of bolts under tensile loading can be well predicted as illustrated in Fig. 8. However, fracture of bolts under tensile loading cannot be estimated if the fracture behaviour of bolt material is not considered in numerical analysis. In last decades, the Void Growth Model (VGM) has been developed to predict the ductile damage and fracture of materials based on the relationship between the growth rate of voids and stress triaxiality [14–17], which is an exponential function found by Rice and Tracey through analysing a spherical void in a simple tension strain rate field [32]. The VGM will be used to predict the fracture of the bolts under tensile loading.

In the VGM, material fracture is predicted to occur when the Void Growth Index (*VGI*) gets to a critical value, VGI_{critical}. This corresponds to the voids growing large enough to trigger necking instabilities between voids resulting in coalescence and macrocrack formation [14–17]. In the following analysis, the VGM based on the Rice-Tracey function is denoted as RT fracture criterion, which is a function of fracture equivalent plastic strain to stress triaxiality as expressed in Eq. (5).

$$\bar{\varepsilon}_f(\eta) = \alpha \cdot exp(\beta \cdot \eta) = 2.0 \cdot exp(-1.5 \cdot \eta) \tag{5}$$

In Eq. (5), $\bar{\varepsilon}_f$ is the fracture equivalent plastic strain. η denotes the stress triaxiality equal to $-p/q$, in which p and q are pressure stress and Mises equivalent stress, respectively. α and β are two material constants. β is generally taken as −1.5 [14–17], while α is similar to VGI_{critical} in the VGM and can be taken as 2.0 according to the experimental calibration conducted by Džugan et al. [33] for ferritic steels.

4.2. BW fracture criterion

Bao and Wierzbicki [18,19] conducted a series of tests including compression tests, shear tests, and tension tests on aluminium alloy. It is concluded that for negative stress triaxiality, fracture is governed by shear mode. For larger stress triaxiality, void growth is the dominant failure mode, while at stress triaxiality between above two regimes, fracture may develop as a combination of shear and void growth modes. The fracture criterion proposed by Bao and Wierzbicki is denoted as BW fracture criterion, which is a function of fracture equivalent plastic strain to stress triaxiality as expressed in Eq. (6).

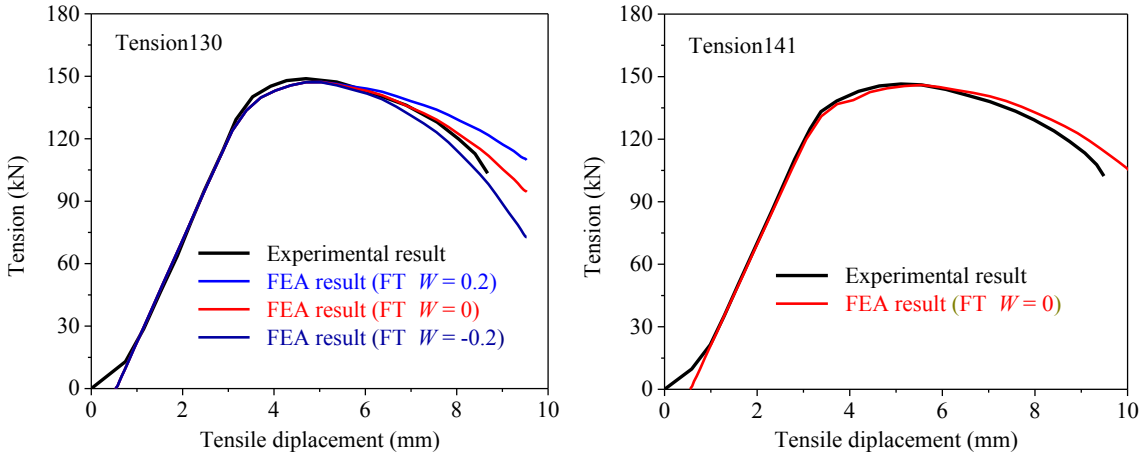

a) Tension130 specimen b) Tension141 specimen

Fig. 8. Calibration of bolt post-necking stress–strain relations.

$$\bar{\varepsilon}_f(\eta) = \begin{cases} \infty, \eta < -1/3; \\ \dfrac{C_1}{3\eta + 1}, -1/3 \leqslant \eta < 0; \\ (C_2 - C_1)(\eta/\eta_0)^2 + C_1, 0 \leqslant \eta < \eta_0; \\ \dfrac{C_2}{\eta/\eta_0}, \eta_0 \leqslant \eta. \end{cases} \tag{6}$$

In Eq. (6), C_1 and C_2 are two material constants governing the shear fracture and tensile fracture behaviour and can be calibrated based on pure shear test and uniaxial tension test, respectively.

Fig. 9 illustrates the dependence of fracture equivalent plastic strain (PEEQ) on stress triaxiality in RT and BW fracture criteria. For the BW fracture criterion, η_0 can be taken as 1/3 corresponding to the stress triaxiality under pure axial tension, since the fracture PEEQ at the pure tension state could get to the maximum value. As illustrated in Fig. 9, two constants C_1 and C_2 determine the fracture PEEQ at each stress triaxiality. Although the BW fracture criterion is put forward based on tests on aluminium alloy, this fracture criterion could also be used to simulate the fracture of steel material through calibrating material constants C_1 and C_2. Hai et al. [34] recently reported a numerical simulation on cyclic loading experiments of S690 high strength steel beam-columns bending about strong axis. The BW fracture criterion was incorporated in the numerical simulation. The simulated hysteretic curves and failure modes both provide good agreements with the experimental results. Song et al. [35] recently reported a comprehensive

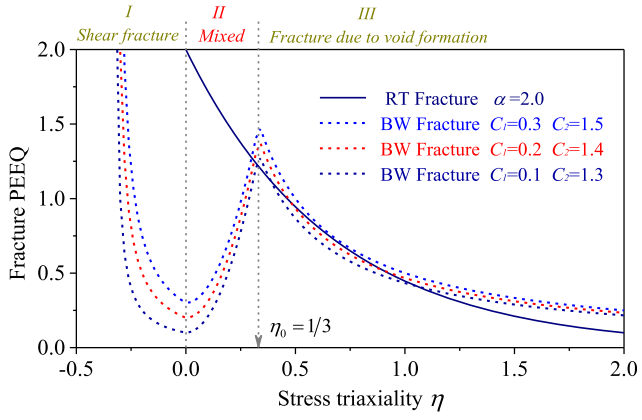

Fig. 9. Dependence of fracture PEEQ on stress triaxiality (RT and BW fracture criteria).

study on the behaviour of austenitic stainless bolts under combined tension and shear. The BW fracture criterion was calibrated to simulate the bolt behaviour under pure tension and shear. Reasonable predictions for bolt fracture behaviours were obtained. In the following analysis, material constants for bolts will be calibrated according to pure tension and shear tests.

For steel fracture simulation using ABAQUS [23], steel fracture is realized through defining damage initiation criterion and damage evolution law. Only the fracture modes of bolts are concerned in this study, excluding the investigation on crack evolution or fracture process of bolts. Therefore, the above RT and BW fracture criteria are taken as the damage initiation criterion. Damage evolution law is defined by the displacement type with a very small displacement at failure, such as 0.001, to achieve the sudden fracture shortly after the damage initiation. Detailed description for investigation of the fracture process with the energy-based approach can be found in [33,36]. Damage initiation will occur when the condition expressed by Eq. (7) is satisfied.

$$\omega_f = \int \frac{d\bar{\varepsilon}^{pl}}{\bar{\varepsilon}_f(\eta)} = 1 \tag{7}$$

In Eq. (7), ω_f denotes the damage index, $\bar{\varepsilon}^{pl}$ is the equivalent plastic strain (PEEQ), and $\bar{\varepsilon}_f(\eta)$ is the fracture PEEQ as expressed by Eqs. (5) and (6). Here, "damage" can be understood as "fracture" since the fracture is very close to the initial damage in the numerical analysis of this paper.

4.3. Fracture criteria calibration

Two material constants in the BW fracture criterion needs to be calibrated for the fracture simulation of bolts under tensile loading. In the study by Pavlović [37], tension and pure shear tests were conducted on M24 grade 8.8 bolts. Tension and pure shear tests are simulated here to validate the RT fracture criterion and calibrate the BW fracture criterion. The tensile coupon has a 10 × 4 mm rectangular cross-section in the gauge part and the parallel length is 44 mm. Firstly, the post-necking stress–strain relation is calibrated based on the combined linear and power stress–strain law expressed as Eq. (3). It indicates that the combined stress–strain law with weighting factor $W = 0$ describes the post-necking behaviour of M24 bolt material very well, as shown in Fig. 10a. The RT fracture criterion and the BW fracture criterion with C_2 equal to 1.3, 1.4, and 1.5 are used to simulate the tensile fracture. Fig. 10b illustrates the numerical engineering stress–strain curves compared to the experimental curve. It indicates that both the RT fracture criterion and the BW fracture criterion can accurately simulate the fracture of the tensile coupon. Although only one tensile coupon test reported in the

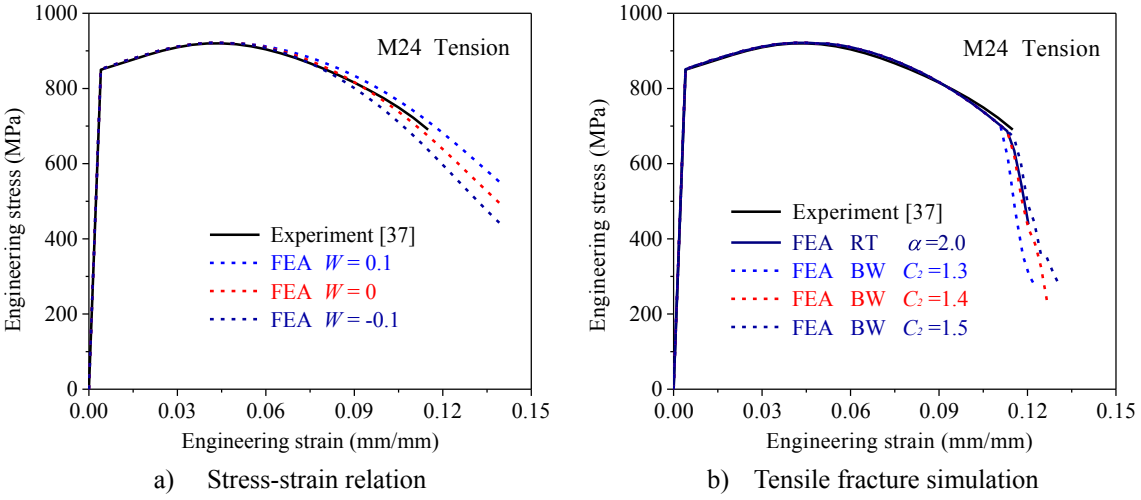

Fig. 10. Calibration of the tensile fracture (Experiment from [37]).

study by Pavlović [37] is used to calibrate the post-necking behaviour of M24 bolt material, results shown in Fig. 10a still verify that the post-necking behaviour of bolt material can be described by Eq. (3) with $W = 0$, same as the investigated PT bolts in this paper. The validity of the calibrated parameters in fracture criteria will be discussed further in the following fracture simulation of PT bolts.

Fig. 11 shows the deformation and PEEQ contour plots of the tensile coupon after the initial fracture governed by RT fracture criterion and BW fracture criterion with $C_2 = 1.4$. The tensile fracture initiates from the core of the critical necking region. Using the BW fracture criterion with $C_2 = 1.4$, fracture of the tensile coupon could be predicted almost the same as using the RT fracture criterion. The maximum PEEQ locates in the core of the critical necking region and has a value of about 0.86 under both fracture criteria. This is because the average stress triaxiality is about 0.5 in the core of the critical necking region, and the fracture PEEQ governed by the BW fracture criterion with $C_2 = 1.4$ is close to that governed by RT fracture criterion for the tensile coupon, as shown in Fig. 9. Therefore, the BW fracture criterion with $C_2 = 1.4$ will be adopted in the following analysis.

Shear tests on M24 grade 8.8 bolts implemented in [37] are simulated with the calibrated stress–strain relation and the BW fracture criterion. Fig. 12a shows the numerical compression-displacement curves compared to two experimental curves BS2 and BS3. Plastic stage of the experimental curves can be approximately predicted including the bolt shear strength, while the initial push-out stage cannot be accurately simulated since there are still some differences between the numerical and experimental boundary conditions and friction status. It is evident the shear ductility grows with the increase of material constant C_1. For the unthreaded part of M24 bolts, using BW fracture criterion with $C_1 = 0.30$ gives good approximation for the actual shear failure. Fig. 12b shows the deformation and PEEQ contour plot of the bolt close to shear fracture using the BW fracture criterion with $C_1 = 0.30$, in which the deformation scale factor is 1.0. The bolt will be cut off simultaneously from two shear planes. The PEEQ in the shear planes is the major concern since shear fracture would occur from these regions. The red regions in the shear planes shown in Fig. 12b have PEEQ value as large as 0.3, and the maximum PEEQ 0.824 occurs in hole edges of the push-out plate. Therefore, value of C_1 in the BW fracture criterion represents the maximum PEEQ in the critical shear plane close to fracture.

5. Fracture simulations

5.1. Tension-displacement curves

As mentioned above, thread rolling process for producing the external threads of bolts would introduce large plastic strain in the region of the threads. Domblesky and Feng [25,26] conducted a systematic numerical analysis on the thread rolling process. Two-dimensional plane

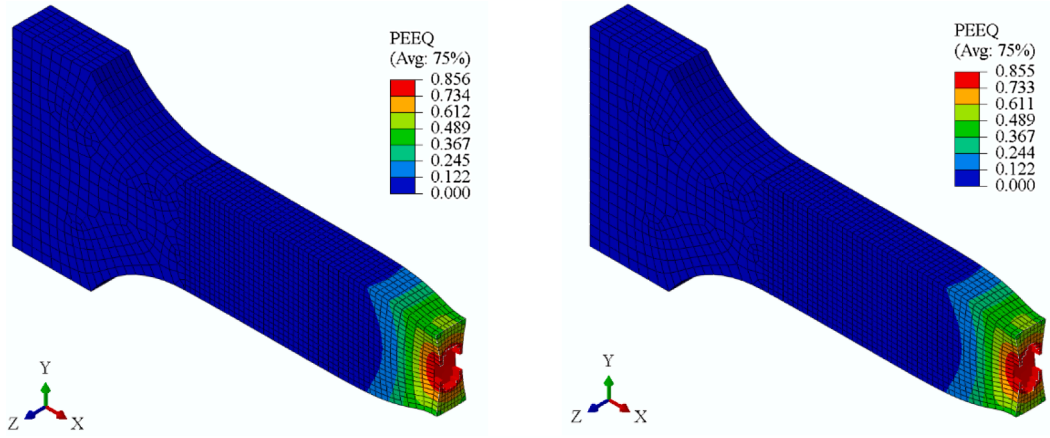

Fig. 11. Deformation and fracture of tensile coupon.

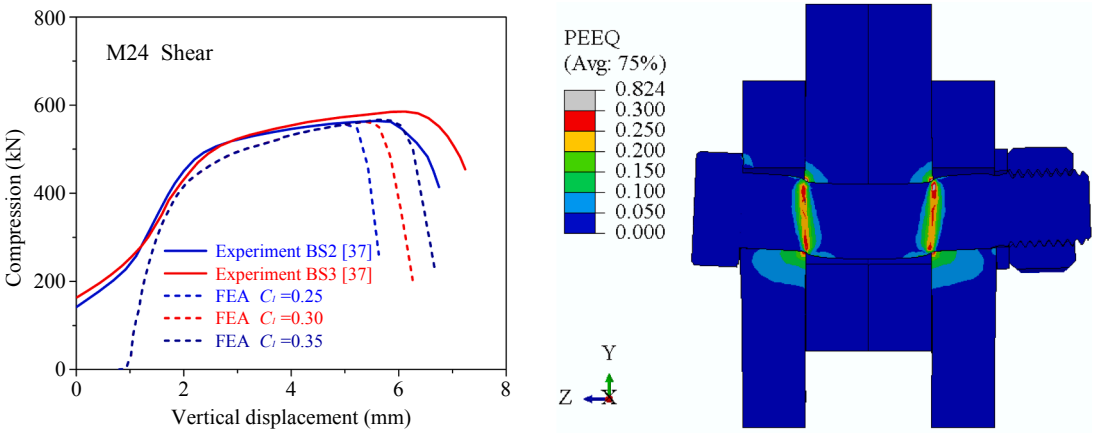

a) Compression-displacement curves b) Deformation and PEEQ contour plot

Fig. 12. Bolt shear fracture simulation using BW fracture criterion (Experiment from [37]).

strain model and three-dimensional model were used to analyse the plastic strain distribution in and after thread rolling. Numerical results indicate that the plastic deformation is concentrated near the thread surface while the shank core is slightly deformed. Measured micro-hardness results also prove that the plastic strain tends to increase from the internal of threads to the crest of threads. The plastic strain in threads around the pitch line would be as large as 0.5–0.8. Therefore, large work hardening effects occur in external threads during the thread rolling process, which would increase the material strength but decrease the material ductility in threads. The fracture PEEQ of threads under external loading will be reduced due to the introduced large plastic strain in thread rolling process. More detailed investigations on thread rolling process have been reported in [27,28].

Given the thread rolling process for forming bolt external threads introduces large plastic strain in thread regions and reduces the thread shear fracture PEEQ, constant C_1 in the BW fracture criterion is reduced and calibrated to predict the thread stripping failure of bolts with a short-threaded length within the grip. The calibrated BW fracture criterion with $C_1 = 0.30$ and $C_2 = 1.4$ is used to simulate the fracture behaviour of nuts since the internal threads of nuts are manufactured by cutting process rather than thread rolling process, without work hardening effects occurring in internal thread regions.

Using the calibrated material properties and fracture criteria, tensile behaviours of PT bolts with various threaded lengths within the grip, as shown in Figs. 1 and 2, are simulated. Fig. 13 exhibits the numerical tension-displacement curves based on RT and BW fracture criteria compared to the corresponding experimental results of PT bolts in tension tests. For Tension118 and Tension122 tests, numerical results based on the BW fracture criteria with $C_1 = 0.10$, 0.15, 0.20, and 0.30 are illustrated. For other three tests, numerical results based on the BW fracture only include $C_1 = 0.10$ and 0.30. Note that there is no available experimental result for Tension126 test in [7], only FEA results are shown in Fig. 13c.

In the experiments of PT bolts under tension [7], all five Tension118 and Tension122 tests exhibit thread stripping failure and all five Tension130 and Tension141 tests have tensile fracture failure. The five experimental tension-displacement curves for each group are almost identical. Whereas three Tension126 tests are thread stripping failure and other two tests are tensile fracture. In the fracture simulations, using the RT fracture criterion would only generate tensile fracture failure for all tests, while using the BW fracture criterion with a small value of C_1 leads to thread stripping failure for Tension118 and Tension122 tests. As shown in Fig. 13a for Tension118 test, tensile deformation capacity of the bolt has a gradually increasing trend as the increase of C_1 in the BW fracture criterion. All failure modes of Tension118 using the BW fracture criterion are thread stripping failure, which will be discussed in detail in the following analysis. For Tension122 test as shown in Fig. 13b, thread stripping failure would occur only when C_1 is equal to 0.1. The failure mode would be altered from thread stripping failure to tensile fracture failure when C_1 is larger than 0.1. For other three tension tests shown in Fig. 13c to 13e, their failure modes are only tensile fracture when C_1 is not less than 0.1 in the BW fracture criterion.

Table 1 lists the comparisons between numerical and experimental results for the investigated PT bolts under tensile loading. The maximum tensile force or tensile resistance of each bolt can be perfectly predicted, see the last column of Table 1. The failure displacement ratios indicate that using BW fracture criterion with $C_1 = 0.1$ can predict the bolt deformation capacity much better than using RT fracture criterion for Tension118 and Tension122 tests with thread stripping failure modes. For Tension130 and Tension141 tests, both the BW fracture criterion with $C_1 = 0.3$ and the RT fracture criterion predict the tensile fracture failure very well, while the BW fracture criterion with $C_1 = 0.1$ would slightly underestimate the force in tension at load-descending stages for Tension130 and Tension141 tests.

5.2. Damage index and PEEQ

Figs. 14–17 illustrate the damage index (DUCTCRT) and equivalent plastic strain (PEEQ) contour plots with real deformations (deformation scale factor equal to 1.0) in the step close to respective fracture for Tension118, Tension122, Tension130, and Tension141. Fig. 14 shows the damage index and PEEQ contour plots of Tension118 using the BW fracture criterion with $C_1 = 0.1$ and $C_1 = 0.3$ and the RT fracture criterion. Different thread failure modes can be clearly seen. When C_1 is set to 0.1 and 0.3 in the BW fracture criterion, the shear fracture of threads governs the final failure of the bolt. The maximum PEEQs equal to 0.1 and 0.3 locate in the shear plane of bolt threads, and the maximum PEEQs in the core of the bolt threaded part about 0.08 and 0.20, respectively. Using the RT fracture criterion, large bending deformation will occur in bolt threads since the fracture PEEQ at the pure shear state is equal to 2.0 in the RT fracture criterion, see Fig. 9. The maximum PEEQ in bolt threads would be as large as 0.8 in the step close to thread failure due to the large bending deformation, which is not consistent with the actual experimental failure mode.

Fig. 15 shows damage index and PEEQ contour plots wither real deformations for Tension122 with $C_1 = 0.1$ and $C_1 = 0.15$ in the BW fracture criterion in the step close to failure. The failure mode of Tension122 would be altered from thread stripping to tensile fracture with C_1 increasing from 0.1 to 0.15. The former is a brittle failure mode while the latter has a certain deformation capacity, see the respective tension-

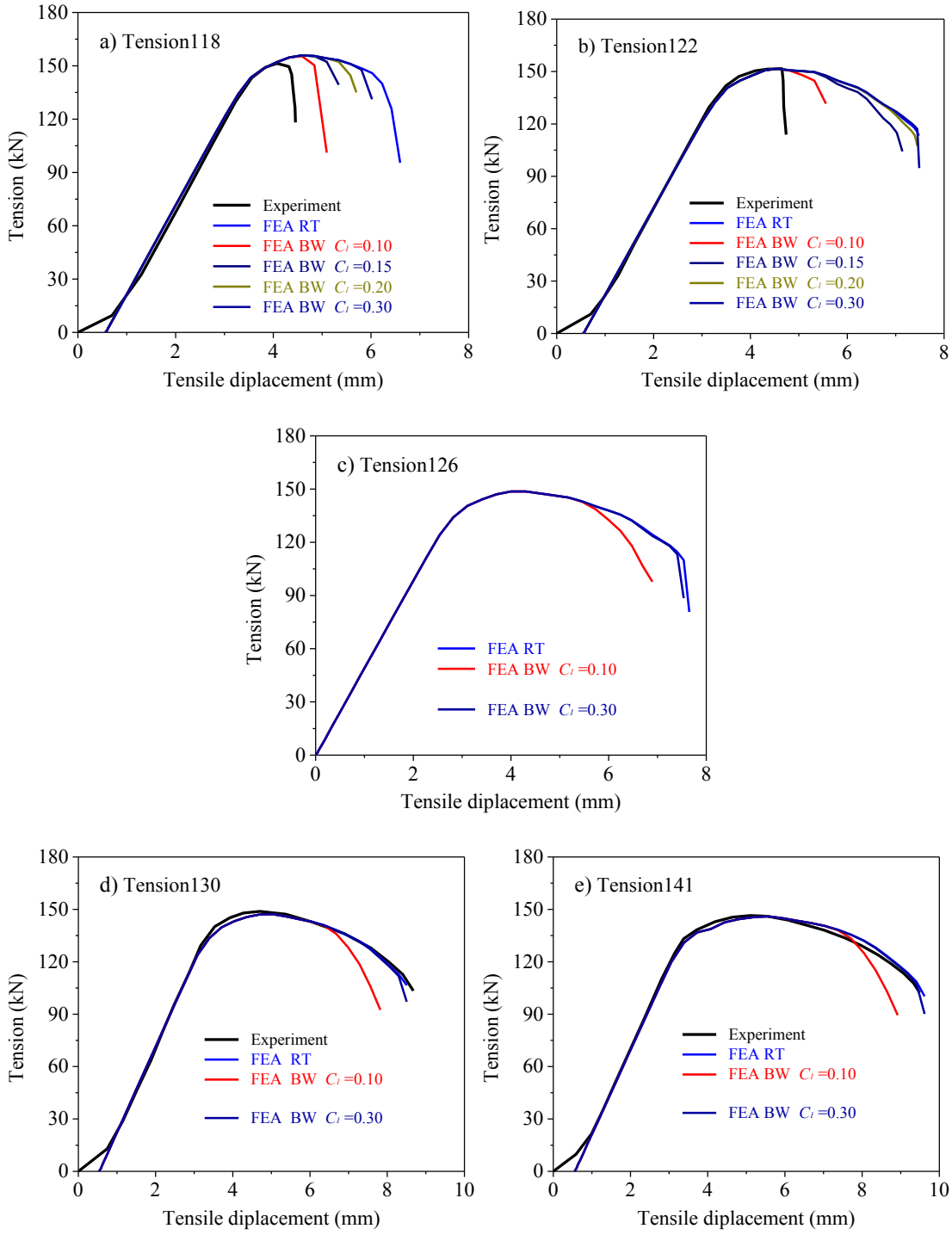

Fig. 13. Numerical tension-displacement curves vs. experimental results.

displacement curves in Fig. 13b. For the tensile fracture failure, necking phenomenon is evident in the step close to fracture and the maximum PEEQ in the core of the bolt threaded part is as large as 0.7, which is not consistent with the actual experimental result. All five tests on Tension122 show the thread stripping failure, it is therefore inferred that the value of C_1 in the BW fracture criterion, governing the thread shear behaviour should be about 0.1. For the thread stripping failure of Tension122, the maximum PEEQ in the core of the threaded part is about 0.2 in the step close to fracture, see Fig. 15c. This means the threaded part within the grip has entered the necking stage but the necking is not significant. The slight necking can also be proved by the damage index value in the core of the threaded part, see Fig. 15a. The necking results in the reduction of bolt diameter in the upper engagement region of bolt and nut. Then the shear area of the bolt first circle thread engaged in the nut is reduced, leading to the increase of PEEQ in bolt threads and eventually triggers the fracture of bolt threads. Given that three Tension126 tests in all five have the thread stripping failure, it is believed that value of C_1 in the BW fracture criterion may be less than 0.1 because the numerical failure of Tension126 is just the tensile fracture.

Figs. 16 and 17 show the damage index and PEEQ contour plots for Tension130 and Tension141 tests with real deformations using the BW fracture criterion with C_1 equal to 0.1 and 0.3. The tensile fracture of

Table 1
Comparisons between numerical and experimental results (Experimental results are).

Test	Failure displacement (mm)					Maximum tension (kN)		
	Experiment (1)	RT fracture (2)	BW fracture * (3)	(2)/(1)	(3)/(1)	*Experiment (4)*	FEA (5)	(5)/(4)
Tension 118	*4.3*	6.23	4.84	1.45	1.13	*151.8*	155.5	1.02
Tension 122	*4.8*	7.48	5.32	1.56	1.11	*152.4*	151.6	0.99
Tension 130	*8.6*	8.51	8.30	0.99	0.97	*149.1*	147.2	0.99
Tension 141	*9.5*	9.62	9.41	1.01	0.99	*147.3*	146.0	0.99

* $C_1 = 0.1$ is used in the simulations of Tension118 and Tension122 tests; $C_1 = 0.3$ is used in the simulations of Tension130 and Tension141 tests.
adopted from [7]

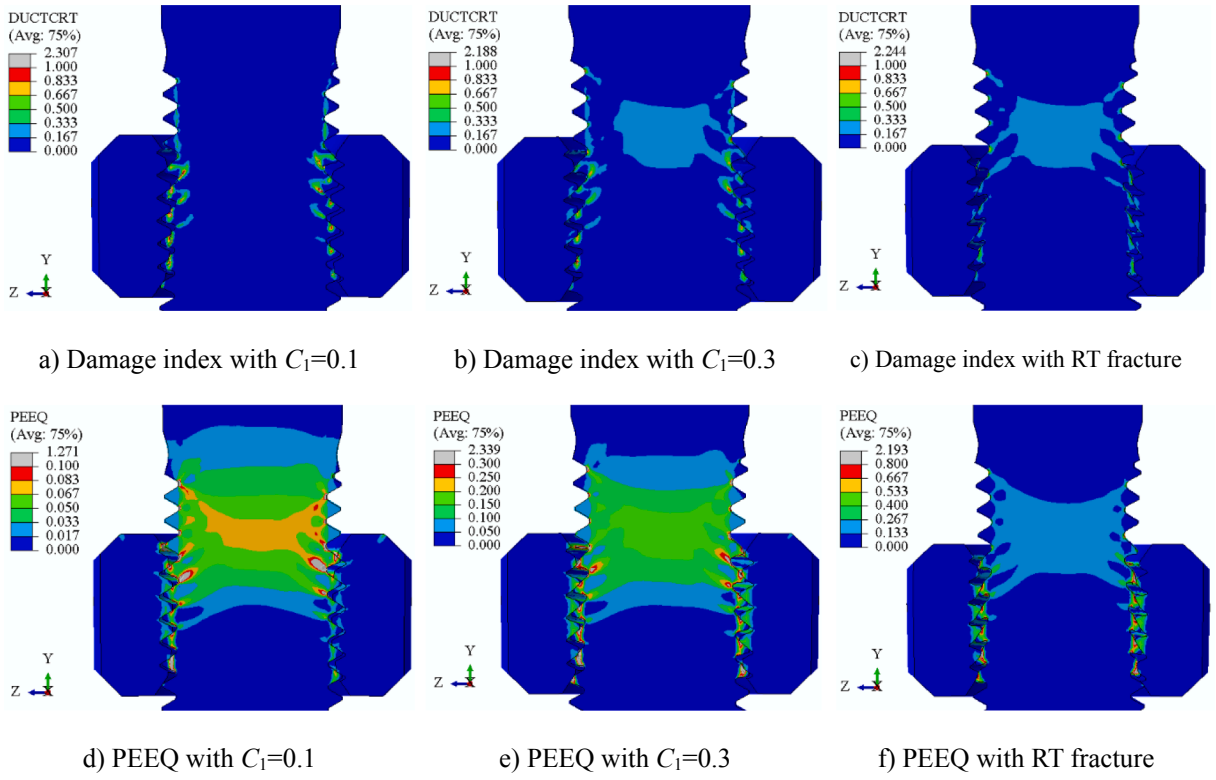

a) Damage index with C_1=0.1 b) Damage index with C_1=0.3 c) Damage index with RT fracture

d) PEEQ with C_1=0.1 e) PEEQ with C_1=0.3 f) PEEQ with RT fracture

Fig. 14. Damage index and PEEQ for Tension118 close to fracture (thread stripping).

Tension130 and Tension141 initiates from the core of the bolt threaded part. The maximum PEEQs in the core of bolt necking regions are as large as 0.8, see Fig. 16c and 17c. This is close to the fracture PEEQ in the uniaxial tensile specimen shown in Fig. 11. It can be seen from Fig. 13 that using the BW fracture criterion with $C_1 = 0.3$ would result in very good predictions for the force in tension at the load-descending stage for Tension130 and Tension141 tests, compared to the respective experimental results. However, if C_1 is set to 0.1 the force in tension at the last load-descending stage is significantly less than the experimental result. It can be explained that using $C_1 = 0.1$ would result in shear fracture of threads in the critical necking region, see Figs. 16a and 17a for Tension130 and Tension141, respectively. The shear fracture of threads in the necking regions lead to the decrease of the tensile force at the load-descending stage. In practise, threads in the necking region would not be cut off from the thread roots, since the plastic strain introduced in the thread root regions in thread rolling process is very small. Results with $C_1 = 0.3$ indicate that the threads in the necking region would not be cut off, see Fig. 16b and 16c for Tension130 and Fig. 17b and 17c for Tension141. Tensile fracture occurs initially from the core of the bolt threaded part for Tension130 and Tension141 tests, as shown Figs. 16c and 17c.

5.3. Failure modes

It can be concluded that using BW fracture criterion could predict two failure modes of PT bolts under tensile loading, thread stripping failure and tensile fracture failure. Fig. 18 shows these two failure modes: thread stripping failure of Tension122 and tensile fracture failure of Tension130. The former is simulated using $C_1 = 0.1$ and the latter uses $C_1 = 0.3$ in the BW fracture criterion. In fact, the thread shear fracture behaviour varies from thread root to thread crest. The shear fracture PEEQ has a decreasing trend from thread root to thread crest as the introduced plastic strain in thread rolling process has an increasing trend from thread root to thread crest. For the failure of Tension122, there is no evident necking phenomenon in the threaded part within the grip. The threads in the engagement length of bolt and nut are sheared off due to the plastic strain growing up to its shear fracture PEEQ around 0.1. For the failure of Tension130, the necking phenomenon is

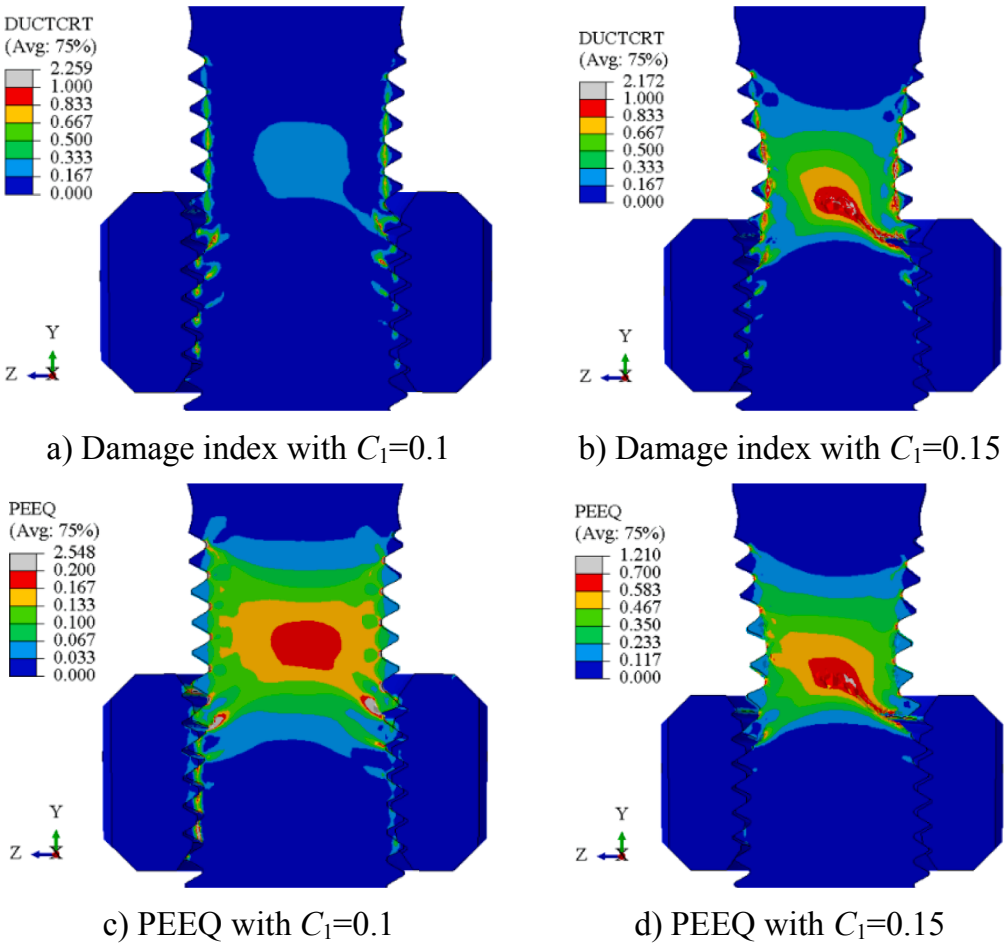

Fig. 15. Damage index and PEEQ for Tension122 close to fracture (thread stripping).

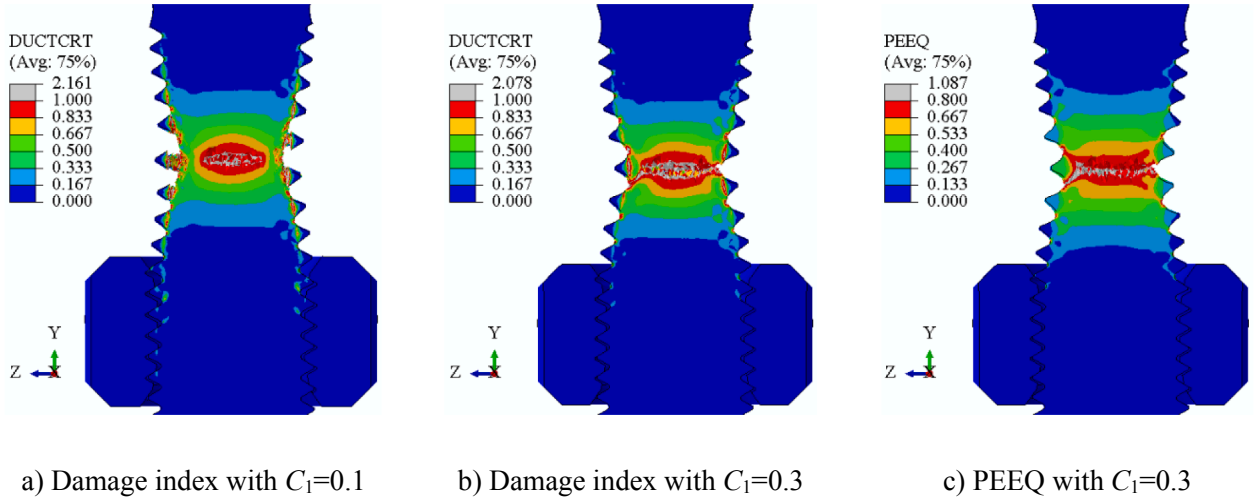

Fig. 16. Damage index and PEEQ for Tension130 close to fracture (Tensile fracture).

significant in the core of the threaded part within the grip, where strain localization occurs seriously and finally the PEEQ grows up to its tensile fracture PEEQ around 0.8.

Note that thread dimensions of bolt and nut could also affect the failure mode of PT bolts under tensile loading. Shear area in the thread engagement region of bolt and nut will be reduced if the clearance between bolt and nut threads gets larger. The risk of bolt threads having a brittle thread stripping failure under tensile loading will increase as the tip of bolt threads has much smaller shear fracture PEEQ.

6. Conclusions

This paper numerically investigated the fracture behaviour of partially threaded bolts under tensile loading with different threaded

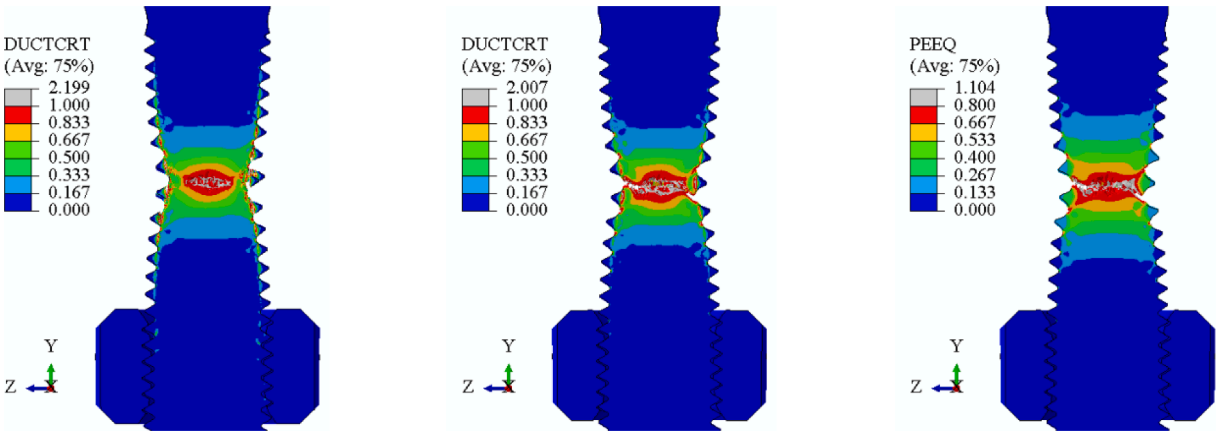

a) Damage index with C_1=0.1 b) Damage index with C_1=0.3 c) PEEQ with C_1=0.3

Fig. 17. Damage index and PEEQ for Tension141 close to fracture (Tensile fracture).

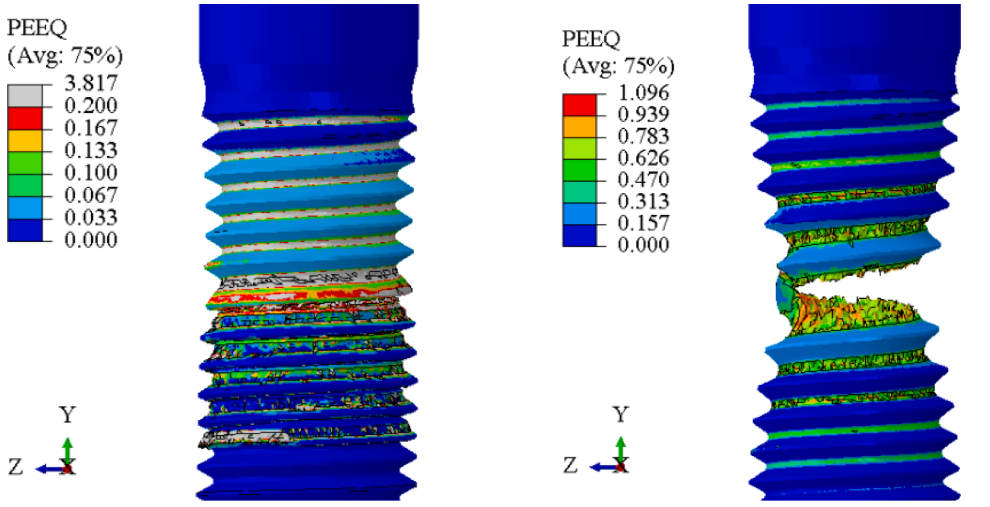

a) Thread stripping for Tension122, C_1=0.1 b) Tensile fracture for Tension130, C_1=0.3

Fig. 18. Failure modes of bolts under tensile loading.

lengths within the grip. Comparison with available experimental results is done. The post-necking stress–strain relations for bolt threaded parts are calibrated and discussed. The Void Growth Model and the fracture criterion proposed by Bao and Wierzbicki are used to simulate the bolt fracture. Following conclusions are drawn from analysis.

(1) The combined linear and power stress–strain law with weighting factor $W = 0$ can be adopted to describe the post-necking stress–strain relation of the investigated partially threaded bolts. It is proved by the good prediction for bolt tensile behaviours especially at the load-descending stage.

(2) The Void Growth Model (denoted as RT fracture criterion) with the critical Void Growth Index equal to 2.0 yields excellent prediction for the tensile fracture of bolts with large threaded lengths within the grip. However, the RT fracture criterion cannot successfully predict the thread stripping failure of bolts, because the fracture equivalent plastic strain corresponding to pure shear state in the RT fracture criterion is as large as 2.0, extremely overestimating the shear fracture of bolt threads.

(3) The BW fracture criterion with $C_1 = 0.3$ and $C_2 = 1.4$ estimates the shear fracture in bolt shank part and the tensile fracture in bolt threaded part very well. Given that thread rolling process for forming bolt external threads introduces large plastic strain in bolt thread regions and reduces the thread shear fracture equivalent plastic strain, constant C_1 in the BW fracture criterion is reduced and calibrated to be 0.1 to make good predictions for the thread stripping failure of bolts with short-threaded lengths within the grip.

(4) For bolts with thread stripping failure, slight necking occurs before the thread stripping failure. The reduction of bolt diameter around the upper engagement region appears and then shear area of the bolt upper threads is reduced. This leads to a growing plastic strain up to the shear fracture equivalent plastic strain around 0.1 and finally triggers the shear fracture of bolt threads. For bolts with tensile fracture failure, the initial tensile fracture occurs in the core of the bolt threaded part with the tensile fracture equivalent plastic strain around 0.8.

CRediT authorship contribution statement

Fei Yang: Visualization, Methodology, Investigation, Validation, Formal analysis, Writing - original draft. **Milan Veljkovic:** Resources, Supervision, Writing - review & editing. **Yuqing Liu:** Conceptualization, Supervision, Writing - review & editing.

Declaration of Competing Interest

The author declare that there is no conflict of interest.

Acknowledgements

The first author would like to acknowledge the financial support provided by the China Scholarship Council (CSC) [Grant number: 201806260196].

References

[1] EN 1993-1-8, Design of steel structures, Part 1-8: Design of joints, European Committee for Standardization, Brussels, Belgium; 2005.
[2] Girao CAM, Bijlaard FSK, Simoes da Silva L. Experimental assessment of the ductility of extended end plate connections. Eng Struct 2004;26(9):1185–206.
[3] Løhre GE, Holm CA, Magnus L, et al. An experimental study of static and dynamic behaviour of bolted end-plate joints of steel. Int J Impact Eng 2015;85:132–45.
[4] Moore AM, Rassati GA, Swanson JA. Evaluation of the current resistance factors for high-strength bolts. University of Cincinnati 2008.
[5] Anja R, Jörg L. Load-bearing behaviour of high-strength bolts in combined tension and shear. Steel Construction 2012;5(3):151–7.
[6] Fransplass H, Langseth M, Hopperstad OS. Tensile behaviour of threaded steel fasteners at elevated rates of strain. Int J Mech Sci 2011;53(11):946–57.
[7] Løhre GE, Arne A, Magnus L, et al. Failure modes of bolt and nut assemblies under tensile loading. J Constr Steel Res 2016;126:15–25.
[8] Kanvinde AM, Deierlein GG. Finite-element simulation of ductile fracture in reduced section pull-plates using micromechanics-based fracture models. J Struct Eng 2007;133(5):656–64.
[9] Kanvinde AM. Predicting fracture in civil engineering steel structures: State of the art. J Struct Eng 2016;143(3):03116001.
[10] Amadio C, Bedon C, Fasan M, et al. Refined numerical modelling for the structural assessment of steel-concrete composite beam-to-column joints under seismic loads. Eng Struct 2017;138:394–409.
[11] Hooputra H, Gese H, Dell H, et al. A comprehensive failure model for crashworthiness simulation of aluminium extrusions. Int J Crashworthiness 2004;9 (5):449–64.
[12] Achouri M, Germain G, Dal Santo P, et al. Experimental characterization and numerical modeling of micromechanical damage under different stress states. Mater Des 2013;50:207–22.
[13] Noell PJ, Carroll JD, Boyce BL. The mechanisms of ductile rupture. Acta Mater 2018;161:83–98.
[14] Kanvinde AM, Deierlein GG. The void growth model and the stress modified critical strain model to predict ductile fracture in structural steels. J Struct Eng 2006;132(12):1907–18.
[15] Jia LJ, Kuwamura H. Ductile fracture simulation of structural steels under monotonic tension. J Struct Eng 2014;140(5):04013115.
[16] Liao F, Wang M, Tu L, et al. Micromechanical fracture model parameter influencing factor study of structural steels and welding materials. Constr Build Mater 2019; 215:898–917.
[17] Han Q, Jiang K, Wen J, et al. Micromechanical fracture models of Q345 steel and its weld. J Mater Civ Eng 2019;31(11):04019268.
[18] Yingbin B, Tomasz W. On fracture locus in the equivalent strain and stress triaxiality space. Int J Mech Sci 2004;46(1):81–98.
[19] Bao Y, Tomasz W. On the cut-off value of negative triaxiality for fracture. Eng Fract Mech 2005;72(7):1049–69.
[20] International Organization for Standardization (ISO), ISO 4014, Hexagon Head Bolts - Product Grades A and B, ISO, Switzerland, 2011.
[21] International Organization for Standardization (ISO), ISO 4032, Hexagon Regular Nuts (Style 1) – Product Grades A and B, ISO, Switzerland, 2012.
[22] Skavhaug Elin Stensrud. Østhus Svanhild Irene. Tension-loaded bolted connections in steel structures. Master's thesis, NTNU 2015.
[23] Abaqus Analysis User's Guide, Version 6.13. Dassault Systèmes Simulia Corp., Providence, RI, USA, 2013.
[24] EN 1090-2: 2018 Execution of steel structures and aluminium structures - Part 2: Technical requirements for steel structures, European Committee for Standardization, Brussels, Belgium.
[25] Domblesky JP, Feng F. Two-dimensional and three-dimensional finite element models of external thread rolling. Proc Instit Mech Eng B: J Eng Manufact 2002; 216(4):507–17.
[26] Domblesky JP, Feng F. A parametric study of process parameters in external thread rolling. J Mater Process Technol 2002;121(2–3):341–9.
[27] Eduard Nitu, Stefan Tabacu, Monica Iordache, et al. Finite element analysis and experimental validation of the wedge rolling process. Proc Instit Mech Eng B: J Eng Manufact 2013;227(9):1325–39.
[28] Philipp Kramer, Peter Groche. Defect detection in thread rolling processes - Experimental study and numerical investigation of driving parameters. Int J Mach Tools Manuf 2018;129:27–36.
[29] Yun Ling. Uniaxial true stress-strain after necking. AMP J Technol 1996;5(1): 37–48.
[30] Yang Fei, Veljkovic Milan. Damage model calibration for S275 and S690 steels. ce/ papers 2019, 3(5-6): 262-271.
[31] Yang Fei, Veljkovic Milan, Liu Yuqing. Ductile damage model calibration for high-strength structural steels. (Revision submitted).
[32] Rice JR, Tracey DM. On the ductile enlargement of voids in triaxial stress fields. J Mech Phys Solids 1969;17(3):201–17.
[33] Jan Džugan, Miroslav Španiel, Antonín Prantl, et al. Identification of ductile damage parameters for pressure vessel steel. Nucl Eng Des 2018;328:372–80.
[34] Le-Tian Hai, Yanbo Wang, Guoqiang Li, et al. Numerical investigation on cyclic behavior of Q690 high strength steel beam-columns. J Constr Steel Res 2019; 105814.
[35] Yuchen Song, Jia Wang, Brian Uy, et al. Experimental behaviour and fracture prediction of austenitic stainless steel bolts under combined tension and shear. J Constr Steel Res 2020;166:105916.
[36] Ping Xiang, Liangjiu Jia, Ke Ke, et al. Ductile cracking simulation of uncracked high strength steel using an energy approach. J Constr Steel Res 2017;138:117–30.
[37] Pavlović Marko. Resistance of bolted shear connectors in prefabricated steel-concrete composite decks. 2013.